Available online at www.sciencedirect.com
ScienceDirect
Journal of Solid State Chemistry 180 (2007) 3224–3233
JOURNAL OF SOLID STATE CHEMISTRY
www.elsevier.com/locate/jssc

Syntheses and characterizations of complex perovskite oxynitrides $LaMg_{1/3}Ta_{2/3}O_2N$, $LaMg_{1/2}Ta_{1/2}O_{5/2}N_{1/2}$, and $BaSc_{0.05}Ta_{0.95}O_{2.1}N_{0.9}$

Young-Il Kim*, Patrick M. Woodward

Department of Chemistry, The Ohio State University, Columbus, OH 43210, USA

Received 5 June 2007; received in revised form 27 July 2007; accepted 22 August 2007
Available online 14 September 2007

Abstract

The following complex oxynitride perovskites have been prepared: $LaMg_{1/3}Ta_{2/3}O_2N$, $LaMg_{1/2}Ta_{1/2}O_{5/2}N_{1/2}$, and $BaSc_{0.05}Ta_{0.95}O_{2.1}N_{0.9}$. Synchrotron X-ray powder diffraction analyses show that $LaMg_{1/3}Ta_{2/3}O_2N$ and $LaMg_{1/2}Ta_{1/2}O_{5/2}N_{1/2}$ are isostructural to the oxide $La_2Mg(Mg_{1/3}Ta_{2/3})O_6$ (space group $P2_1/n$), whereas $BaSc_{0.05}Ta_{0.95}O_{2.1}N_{0.9}$ has a simple cubic symmetry similarly to $BaTaO_2N$. The orderings of octahedral cations are markedly diminished in the above oxynitrides, as compared with the related oxides such as $La_2Mg(Mg_{1/3}Ta_{2/3})O_6$ and Ba_2ScTaO_6. The optical band gaps are similar for the homologous compositions, $LaMg_{1/3}Ta_{2/3}O_2N$, $LaMg_{1/2}Ta_{1/2}O_{5/2}N_{1/2}$ and $LaTaON_2$ (1.9 eV), and $BaSc_{0.05}Ta_{0.95}O_{2.1}N_{0.9}$ and $BaTaO_2N$ (1.8 eV), while the absorption edges become broader for the complex derivatives. As revealed from the impedance spectroscopic analysis, the oxynitrides have clearly different dielectric components from those of comparable oxides containing Ta^{5+}. Impedance spectroscopy reveals interesting capacitor geometry in $BaSc_{0.05}Ta_{0.95}O_{2.1}N_{0.9}$ in which the semiconducting oxynitride grains are separated by insulating secondary phases. Most notably $BaSc_{0.05}Ta_{0.95}O_{2.1}N_{0.9}$ has a bulk component with a high relative permittivity ($\kappa = 7300$) and the grain boundary component with an even higher κ.

Keywords: Complex perovskite; Oxynitride perovskite; Dielectric; Cation ordering; Pigment

1. Introduction

Complex oxides have supplied numerous materials of interest to solid-state chemists, condensed matter physicists, and materials scientists. To continue extracting novel materials from the oxide family it is necessary to explore compounds with increasing compositional complexity. One promising area is that of mixed anion compounds. In a number of cases the lattice oxygen can be partially replaced by a halogen [1,2], a chalcogen [3,4], or nitrogen [5–8] leading to modifications of the crystal and electronic structures. Thus obtained mixed anion compounds exhibit appreciably distinct but still comparable physical properties to those of pure oxides. Since the perturbations by anionic substitutions are generally greater than the cationic substitutions, one can pursue material design in either rational or explorative ways.

To maintain a three-dimensional structure, oxynitrides and oxyfluorides are regarded to be the most feasible mixed anion systems, due to the similarity of the ionic radii of F^- and N^{-3} to O^{-2} [9]. Previously reported oxynitrides and oxyfluorides are structurally diverse encompassing perovskite, pyrochlore, fluorite, Ruddlesden–Popper, spinel, and scheelite types among others. In contrast the oxychalcogenides or oxychlorides are rarely found in isostructural forms with the respective oxides. These compounds favor layer structures due to the size mismatch between anions.

The perovskite family is arguably the most important oxide structure type. The oxide AMO_3 group includes a large number of compositions owing to the abundance of $A^{m+}-M^{n+}$ pairs that simultaneously satisfy the criteria for the size ratio ($d_{A-O}/d_{M-O} \approx 1$) and valence sum ($m+n=6$). Unfortunately the need to meet both charge and size requirements places some limitations on the number of mixed anion perovskites that can be prepared.

*Corresponding author. Present address: Materials Research Laboratory, University of California, Santa Barbara, CA 93106-5121, USA. Fax: +1 805 893 8797.
E-mail address: ykim@mrl.ucsb.edu (Y.-I. Kim).

0022-4596/$ - see front matter © 2007 Elsevier Inc. All rights reserved.
doi:10.1016/j.jssc.2007.08.031

To illustrate this point consider the effect of replacing O^{-2} ions with N^{-3} ions. The increased charge of the nitride ion requires a corresponding valence increase in one or both of the cations, while at the same time the larger size of the nitride ion favors incorporation of larger cations. The requirements to increase both the size and valence of the cation(s) are generally in conflict with each other. A similar conflict occurs in oxyfluoride perovskites.

The synthetic conditions needed to prepare $AM(O,N)_3$ or $AM(O,F)_3$ compositions also raise challenges. The oxynitrides, which need cations with higher oxidation states, are usually prepared in reductive atmosphere, while for the oxyfluorides the situation is reversed. These considerations may explain in part why there are not more of multinary solid structures with mixed anions. A thorough literature review (see Table 1) reveals that the existing ternary oxynitrides are composed of electropositive cations. Under most nitridation conditions, those transition metals with intermediate electronegativity (W, Mo, V) tend to undergo partial reductions unless they form structures containing isolated polyhedra, whereas the post-transition metals (Cd, In, Sb, Pb, Bi) tend to be reduced to their elemental forms. Of course these statements are generalizations and it may be possible to overcome these trends if the proper synthetic pathways can be identified. For example, computational studies predict that VON can be prepared under the right conditions [48], although to our knowledge this has not yet been experimentally achieved.

Among the effects of compositional variation on the anion site, two prominent impacts can be emphasized. First, the newly introduced anion species can significantly modify the electronic structure of the parent oxide primarily at the valence band. Particularly the oxynitrides have clearly distinguished band gap range and visual colors from the oxides of isoelectronic d^0 configuration. Depending on the cation composition, the oxynitrides display various colors ranging from white to yellow to red to dark brown, which has an implication to the pigment applications. Most of the currently used pigment materials contain hazardous components (Cd, Pb, Cr, Hg, etc.) that are no longer suitable for many commercial applications [49], for which the oxynitrides are considered promising substitutes. A previous study on the solid solution of $LaTaON_2$ and $CaTaO_2N$ demonstrated the prospect for the non-toxic inorganic pigments utilizing the oxynitride compounds [6]. Depending on the composition of $Ca_{1-x}La_xTaO_{2-x}N_{1+x}$ ($x = 0.05$–1), gradual variations of band gap and colors were realized; from $x = 0.05$ (2.75 eV, yellow) to $x = 1$ (2.00 eV, red) [6].

Second, the aliovalent substitutions to derive mixed anion systems will cause significant alteration of the polarization field within the crystal. Being formed of ions with larger valence magnitudes, the oxynitride phases may exhibit markedly enhanced dielectric polarizations, compared with the pristine oxides. In addition the presence of multiple anion types can provide a non-uniform chemical environment for the polarizing cations, thereby affecting the cooperative dipole alignments within the crystal. In fact, unusual dielectric behaviors of $BaTaO_2N$ and $SrTaO_2N$ have recently been reported [8,50–52]. From the polycrystalline samples of $BaTaO_2N$ and $SrTaO_2N$, dielectric constants in excess of 3000 were measured with very weak temperature dependences. Also epitaxial thin films of $BaTaO_2N$ were shown to possess high dielectric constants and a near-zero temperature coefficient [50].

In this work we explore the optical and dielectric properties of complex perovskite oxynitrides $A(M',M'')(O,N)_3$ having two different cations at the octahedral site. Taking into account of atomic attributes such as electronegativity, valence, size, as well as potential competing phases, the most promising cation types for complex perovskite oxynitrides can be narrowed down to La^{3+} and Ba^{2+} for A-site, Mg^{2+} and Sc^{3+} for the M'-site, and Ta^{5+} for M''-site. For the two systems $LaMg_xTa_{1-x}O_{1+3x}N_{2-3x}$ and $BaSc_xTa_{1-x}O_{2+2x}N_{1-2x}$, the multilateral effects of mixed O/N anion on the cation order, band gaps, and dielectric properties are investigated and compared to the analogous complex oxides.

2. Experimental

The oxynitride samples were prepared by the high temperature ammonolysis reactions using high purity powder reagents of $BaCO_3$, La_2O_3, MgO, Sc_2O_3, and Ta_2O_5. Lanthanum and magnesium oxides were baked at 900 °C for 10 h before use. Aiming at the oxynitride compositions of $BaSc_{1/3}Ta_{2/3}O_{8/3}N_{1/3}$, $LaMg_{1/2}Ta_{1/2}O_{5/2}N_{1/2}$, and $LaMg_{1/3}Ta_{2/3}O_2N$, the reagents were appropriately mixed in acetone using agate mortar and pestle. The reactant mixture was heated in an NH_3 gas stream (Praxair, 99.99%) at 830–1000 °C for 15 h, with heating/cooling ramps of 10 °C/min. The ammonolysis heating cycle was repeated with intermittent grindings and the phase identification was examined using X-ray powder diffraction (XRPD). For the $Ba(Sc,Ta)(O,N)_3$ phase, an XRPD single phase could be obtained after ~45 h of reaction, but the two $La(Mg,Ta)(O,N)_3$ perovskite phases seemed to form equilibrium mixtures with small amounts of secondary components such as La_2O_3 and La_3TaO_7 under the experimental conditions of 850–1100 °C and $p(NH_3)$~1 atm. Considerable X-ray peak broadenings also made it difficult to judge the single-phase formation of these complex oxynitrides. Therefore, attempts to form $LaMg_{1/3}Ta_{2/3}O_2N$ and $LaMg_{1/2}Ta_{1/2}O_{5/2}N_{1/2}$ were concluded at the points the diffraction peaks from La_2O_3 and La_3TaO_7 were minimized.

The powder morphology and cation compositions of $Ba(Sc,Ta)(O,N)_3$ and $La(Mg,Ta)(O,N)_3$ samples were examined using a JEOL JSM-820 scanning electron microscope (SEM) with an Oxford eXL energy dispersive X-ray analyzer (EDX). The specimens for SEM–EDX were prepared by spreading the sample powder on conducting carbon adhesive tape. For determining the nitrogen

Table 1
Ternary oxynitrides[a] reported in journals until the mid of year 2007

Structure type	Composition	Precursors[b] and temperature for ammonolysis	Refs.
Perovskite	$BaTaO_2N$	Reagents, 1000 °C/ BaO + TaON, 1500 °C[c]	[10–13]
	$SrTaO_2N$	Reagents, 900–1000 °C/ SrO + TaON, 1500 °C[c]	[10,13,14]
	$CaTaO_2N$	Reagents, 1000 °C/Reagents + mineralizer, 850 °C	[10,14]
	$Ba_{1-x}Sr_xTaO_2N$	$BaTaO_2N + SrTaO_2N$, 950 °C	[15]
	$LaTaON_2$	$LaTaO_4$, 950 °C/Reagents + mineralizer, 850 °C	[16,14]
	$LnTaON_2$	(Ln = Nd, Sm, Gd, Eu) $LnTaO_4$, 950 °C	[16]
	$A_{0.5}La_{0.5}TaO_{1.5}N_{1.5}$	(A = Ba, Sr, Ca) Reagents, 1000 °C	[17]
	$Ca_{1-x}La_x\ TaO_{2-x}N_{1+x}$	(x = 0.05–1.0) Reagents + mineralizer, 850 °C	[6]
	$BaNbO_2N$	Reagents, 1000 °C	[10,11]
	$SrNbO_2N$	Reagents, 1000 °C	[10]
	$CaNbO_2N$	$Ca_2Nb_2O_7$, 730 °C	[8]
	$Sr_2Nb_2O_{7-x}N_x$	(x = 1.5–2.8) $Sr_2Nb_2O_7$, 700–1000 °C	[18]
	$LaNbON_2$	$LaNbO_4$, 950 °C	[16]
	$LaTiO_2N$	$La_2Ti_2O_7$, 950 °C	[16,19]
	$NdTiO_2N$	$Nd_2Ti_2O_7$, 950 °C	[19]
	$LaZrO_2N$	$La_2Zr_2O_7$ fine particle, 900–1000 °C	[19]
	$AZr_xTa_{1-x}O_{2+x}N_{1-x}$	(A = Ba, Sr, Ca) ACO_3 + Ta-Zr-O gel, 1000 °C	[20]
	$SrWO_{1.7}N_{1.3}$	$SrWO_4$, 950 °C	[21]
	$SrWO_2N$	$SrWO_4$, 900 °C	[22]
	$SrMoO_{2.5}N_{0.5}$	$SrMoO_4$, 800 °C	[22]
	$SrMoO_{2.6}N_{0.4}$	$SrMoO_4$, 750 °C	[23]
	$LaWO_xN_{3-x}$	(x = 0.6, 0.7) $La_2W_2O_9$, 700–900 °C	[24,25]
	$NdWO_{0.8}N_{2.2}$	$Nd_2W_2O_9$, 700–900 °C	[25]
	$EuWO_{1.58}N_{1.42}$	$Eu_2W_2O_7$, 850 °C	[26]
	$LaVO_{3-x}N_x$	(x = 0–0.9) $LaVO_4$, 700–800 °C	[27]
Pyrochlore	$Ln_2Ta_2O_5N_2$	(Ln = Nd–Yb, Y) $LnTaO_4$, 950 °C	[28,29]
	$Sm_2Mo_2O_{3.8}N_{3.2}$	$Sm_2Mo_2O_7$, 625 °C	[30]
	$Y_2Mo_2O_{4.5}N_{2.5}$	$Y_2Mo_2O_7$, 625 °C	[31]
Ruddelesden–Popper	A_2TaO_3N	(A = Ba, Sr, Ca) Reagents, 900–950 °C	[32,33]
		(A = Ba, Sr) $2AO$ + TaON, 1500 °C[c]	[13]
	Nd_2AlO_3N	Nd_2O_3 + AlN, 1350 °C[c]	[34]
	$SrO(SrNbO_{2-x}N)_n$	(n = 1, 2) Reagents, 900–1050 °C	[35]
Spinel	$Mn_2MnTa_3N_{6-x}O_{2+x}$	(x = 0–1) Ta-O gel + $Mn(OAc)_2 \cdot 4H_2O$, 902 °C	[36]
	$(Mg,Al)_{3-\delta}(O,N)_4$	Al_2O_3 + AlN + MgO, 1450 °C[c]	[37]
	$Zn_{1.33}Ti_{1.33}O_{4-x-\delta}N_x$	Zn-Ti-O gel, 550–750 °C	[38]
Scheelite	$KOsO_3N$	KOH + OsO_4 + NH_4OH, rt[c]	[39]
	$RbOsO_3N$	$KOsO_3N$ + RbCl, rt[c]	[40]
	$LnWO_3N$	(Ln = Nd, Pr) Ln-W-O gel, 550–700 °C	[41]
Others[d]	Na_3WO_3N	$Na_2WO_4 \cdot 2H_2O$, 700 °C	[42]
	$NaMoO_3N$	MoO_3 + Na_3N, 650 °C	[43]
	Ba_3ZnN_2O	Ba + ZnO + NaN_3 + Na, 750 °C[c]	[44]
	$Ba_3W_2O_6N_2$	$Ba_3W_2O_9$, 800 °C	[45]
	$Ba_3W_2O_{6.3}N_{1.7}$	Reagents, 900 °C	[21]
	$Ba_3Mo_2O_6N_2$	Reagents, 850 °C	[21]
	$CsOsO_3N$	$KOsO_3N$ + CsCl, rt[c]	[46]
	Ba_2VO_3N	Ba-V-O gel, 900 °C	[47]

[a]"Ternary oxynitrides" denotes the compounds containing two different types of cation centered polyhedra.
[b]"Reagents" denotes the mixture of carbonates for alkaline earth and oxides for transition metal or lanthanides.
[c]Non-ammonolytic conditions, heating under N_2 or in an evacuated container, or ion exchange at rt.
[d]Uncommon structure types with isolated polyhedra of transition metal centers.

content in each oxynitride sample, combustion analyses were conducted at Midwest Microanalysis Laboratory (Indianapolis, Illinois).

For the detailed crystal structure analyses, the synchrotron XRPD patterns were collected at the beam line X7A of National Synchrotron Light Source (Brookhaven National Laboratory) using the X-ray radiation of $\lambda \sim 0.7$ Å. In the X7A station with the storage ring current of 2.5 GeV and 250–300 mA, a Ge 111 channel cut crystal monochromator was used and the wavelength was calibrated by a CeO_2 standard. Each sample, packed in a 0.2 or 0.3 mm diameter glass capillary, was spun for better

powder averaging in the Debye–Scherer mode measurement. A gas-proportional linear position sensitive detector was stepped in 0.25° intervals between 3° and 65° to produce 0.01° step scan data. The X-ray diffraction patterns were analyzed either by Le Bail whole pattern fitting ($La(Mg,Ta)(O,N)_3$ perovskite phases) or Rietveld refinement ($Ba(Sc,Ta)(O,N)_3$ phase) using the GSAS-EXPGUI software suite [53,54].

Diffuse-reflectance absorption spectroscopy was performed using a scanning double-beam spectrometer (Perkin-Elmer Lambda 20) equipped with a 50 mm integrating sphere (Labsphere). The absorption spectra were recorded in the ultraviolet (UV) to visible light range ($\lambda = 200$–800 nm) with a commercial $BaSO_4$ disk (Labsphere) as the reference. The band gap energies were determined from Shapiro's method [55] of extrapolating the onset of absorption to the wavelength axis.

The dielectric behaviors were studied using an impedance analyzer (Solartron SI1260) over the frequency range 1–10^7 Hz at room temperature. Due to their refractory nature, the sintering of oxynitrides cannot be achieved in the ordinary conditions applicable to the oxides. As the alternative way to densify oxynitride ceramic, cold-isostatic pressing (American Isostatic Press, Columbus, Ohio) was performed on uniaxially pressed pellets. Although the cold-isostatic pressing did not lead to noticeable changes of the packing density, ~55% for all the three oxynitrides, it did lead to significantly better electrical measurements. For the electrode contacts, In–Ga eutectic (Alfa, 99.99%, In:Ga 24.5:75.5 wt%) was rubbed on both faces of the pellets which were placed between Pt plates connected to BNC lead cables. The measured impedance spectra were analyzed by the equivalent circuit method [56] to separately extract the bulk and grain boundary contributions to the electrical behavior.

3. Results and discussion

3.1. Powder morphology and sample composition

The samples were subjected to SEM analysis. The oxynitride grain shapes are roughly isotropic and the crystallites are of a few 100 nm sizes. These microstructural characteristics are common to all three compounds studied here. For each sample the EDX measurements were conducted for 3–5 different spots focusing on single or clustered grains. In case of $La(Mg,Ta)(O,N)_3$ samples, the EDX results were reproducible from different grains examined, and the averaged results were consistent with the respective target cation ratios, La:Mg:Ta = 3.0:1.0:2.1 for $LaMg_{1/3}Ta_{2/3}O_2N$, and La:Mg:Ta = 2.0:0.9:1.0 for $LaMg_{1/2}Ta_{1/2}O_{5/2}N_{1/2}$. However for the $Ba(Sc,Ta)(O,N)_3$ phase, significant scandium-deficiency was observed when the single grains were examined. The Ba:Sc atomic ratio was measured in the range of 1:0.03–1:0.06 from different individual grains. But when a larger area with many grains was probed, the analyzed composition (Ba:Sc:Ta = 3:1.0:2.2) was close to that of the reactants. This result suggests the formation of $BaSc_xTa_{1-x}(O,N)_3$ crystallites with x far less than $\frac{1}{3}$ in the presence of a scandium-rich matrix.

The combustion analyses confirmed the inclusion of nitrogen in all the three compounds. For the $La(Mg,Ta)(O,N)_3$ samples the measured nitrogen contents agreed with the nominal values (shown in parentheses), 4.6 ± 0.3 wt% for $LaMg_{1/3}Ta_{2/3}O_2N$ (4.47 wt%), and 2.5 ± 0.3 wt% for $LaMg_{1/2}Ta_{1/2}O_{5/2}N_{1/2}$ (2.43%). However for the $Ba(Sc,Ta)(O,N)_3$ sample the nitrogen content was determined to be 2.6 ± 0.2 wt%, significantly higher than the expected amount based on the formula $BaSc1_{/3}Ta_{2/3}O_{8/3}N_{1/3}$ (1.46 wt%). Such an inconsistency strongly suggests the formation of an off-stoichiometric product with a composition that strongly deviates from the target stoichiometry of $BaSc_{1/3}Ta_{2/3}O_{8/3}N_{1/3}$. The Rietveld analysis of the XRPD data supports this conclusion.

3.2. Cation ordering in complex oxynitrides

For complex perovskites, the cation ordering and octahedral tilting are two important characteristics that determine the crystal symmetry of the stabilized structure. Comprehensive descriptions of the space group symmetries of complex perovskites can be found elsewhere [57–60]. To analyze the $Ba(Sc,Ta)(O,N)_3$ data, a primitive cubic model was used since there was no indication of superstructure or distortion. Compared with the XRPD pattern of $BaTaO_2N$, the diffraction peaks from $Ba(Sc,Ta)(O,N)_3$ were observed at similar 2θ values with a slight change in the ratio of peak intensities. The $Pm\bar{3}m$ type refinement of $Ba(Sc,Ta)(O,N)_3$ includes a minimal number of variables which converged rapidly.

The cubic cell edge for the $Ba(Sc,Ta)(O,N)_3$ sample was refined to be equal to 4.11455(3) Å. Not surprisingly this value is very similar to the cell edges observed for $BaTaO_2N$ (4.1125 Å) [8] and Ba_2ScTaO_6 (4.1115×2 Å) [61]. This similarity suggests that it is possible to carry out double exchange of $Ta^{5+} + 2N^{-3}$ for $Sc^{3+} + 2O^{-2}$ over a range of compositions leading to a series of compounds with a general formula of $BaSc_xTa_{1-x}O_{2+2x}N_{1-2x}$. However, since Sc and Ta have markedly distinct X-ray scattering powers it is possible to use the peak intensities to estimate the degree of Sc^{3+} incorporation. The tantalum occupancy of the octahedral site refined to a value of 0.950(1), subject to the constraint that the site was fully occupied, corresponding to a composition of $BaSc_{0.05}Ta_{0.95}O_{2.1}N_{0.9}$. If the octahedral site occupancy is set to 0.33Sc plus 0.67Ta, the R_{wp} value is 9.1%. A significant reduction, to a value of $R_{wp} = 7.5\%$, is observed upon allowing the site occupancy to refine (see Table 2). The Rietveld refinement fit of $BaSc_{0.05}Ta_{0.95}O_{2.1}N_{0.9}$ is shown in Fig. 1. The wide deviation between the reactant and product compositions implies the presence of secondary phases like $BaSc_2O_4$, Sc_2O_3, or ScN, but no impurity phases could be detected in the synchrotron XRPD

Table 2
Atomic positional and thermal parameters for $BaSc_{0.05}Ta_{0.95}O_{2.1}N_{0.9}$ by Rietveld refinement of synchrotron XRPD ($\lambda = 0.7021$ Å)[a]

Atom	Position	Occ[b]	x	y	z	U_{iso} (Å^2)[c]
Ba	1*a*	1	0	0	0	0.0048(4)
Sc	1*b*	0.050(1)	$\frac{1}{2}$	$\frac{1}{2}$	$\frac{1}{2}$	0.0040(3)
Ta	1*b*	0.950(1)	$\frac{1}{2}$	$\frac{1}{2}$	$\frac{1}{2}$	0.0040(3)
O	3*c*	0.7	0	$\frac{1}{2}$	$\frac{1}{2}$	0.007(1)
N	3*c*	0.3	0	$\frac{1}{2}$	$\frac{1}{2}$	0.007(1)

[a]S. G. $Pm\bar{3}m$; $a = 4.11455(3)$ Å, $V = 69.657(2)$ Å^3. Reliability factors: $R_p = 5.0\%$, $R_{wp} = 7.5\%$, $\chi^2 = 7.4$.
[b]Occupancies were fixed for Ba, O, and N, whereas the Ta and Sc occupancies were constrained as Occ(Ta) + Occ(Sc) = 1.
[c]Constraints were used as U(Ta) = U(Sc), U(O) = U(N).

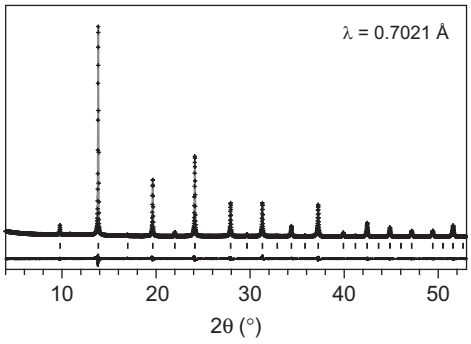

Fig. 1. Rietveld refinement for $BaSc_{0.05}Ta_{0.95}O_{2.1}N_{0.9}$ using a $Pm\bar{3}m$ model with Ba at (0, 0, 0), Sc/Ta at ($\frac{1}{2}$, $\frac{1}{2}$, $\frac{1}{2}$) and O/N at (0, $\frac{1}{2}$, $\frac{1}{2}$). Observed (crosses) and calculated (solid line) patterns are presented together with the difference pattern and the Bragg peak positions at the bottom.

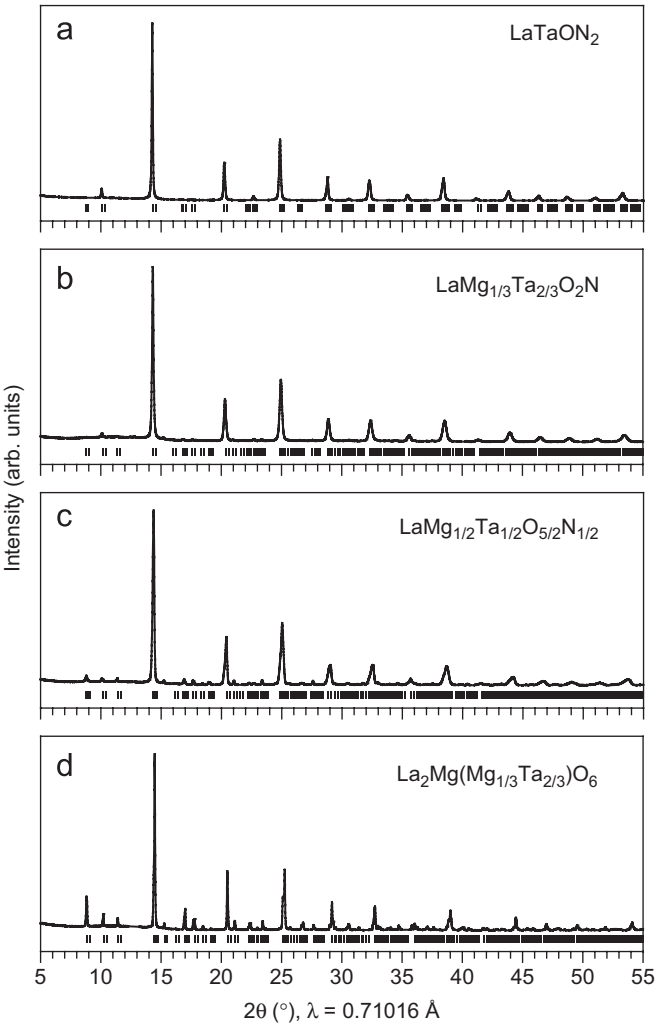

Fig. 2. XRPD patterns of $LaMg_xTa_{1-x}O_{1+3x}N_{2-3x}$ compounds, (a) $x = 0$, (b) $x = \frac{1}{3}$, (c) $x = \frac{1}{2}$, and (d) $x = \frac{2}{3}$. Bragg peak positions are marked according to the refined lattice constants.

pattern. Volatility of barium and/or scandium phases at temperatures below 1000 °C seems unlikely. One plausible model for this behavior is that Sc-rich phase diffused out of bulk to form amorphous shells surrounding crystalline $BaTaO_2N$ grains.

The compositions containing La^{3+} as the *A*-site cation and a mixture of Mg^{2+} and Ta^{5+} on the *B*-site can be considered members of a solid solution with stoichiometry $LaMg_xTa_{1-x}O_{1+3x}N_{2-3x}$. The end members of this solid solution are $LaTaON_2$ and $La_2Mg(Mg_{1/3}Ta_{2/3})O_6$. The XRPD patterns shown in Fig. 2 and structural parameters listed in Table 3 indicate that $LaMg_{1/2}Ta_{1/2}O_{5/2}N_{1/2}$ and $LaMg_{1/3}Ta_{2/3}O_2N$ are intermediate between the end members of this family. All four compounds have monoclinic symmetries due to octahedral tilting distortions. The structure of $LaTaON_2$ has been refined in $C2/m$ space group which occurs from an $a^0b^-c^-$ type tilting [14,61], while the other three compounds could be refined with $P2_1/n$ space group symmetry resulting from $a^-a^-c^+$ tilting and rock salt ordering of *B*-site cations. These phases exhibit a range of cation ordering characteristics (as indicated by the peaks at $d \approx \sqrt{4/3}a_p$, $2\theta \approx 9°$). Complete Mg/Ta ordering was found in $La_2Mg(Mg_{1/3}Ta_{2/3})O_6$ [61], while the cation ordering was markedly reduced in the two oxynitride phases.

From the XRPD peak patterns $LaMg_{1/2}Ta_{1/2}O_{5/2}N_{1/2}$ and $LaMg_{1/3}Ta_{2/3}O_2N$ are regarded isostructural to $La_2Mg(Mg_{1/3}Ta_{2/3})O_6$. However in the Rietveld refinements for the two complex oxynitrides, the high-resolution synchrotron data revealed somewhat broad and asymmetric peak profiles. This peak broadening, which is thought to originate from the cation and anion disorder as well as the corresponding short-range fluctuations in composition, prevented reliable refinements of anion positions. Refinements involving phase separations into the end member compositions were investigated, but we were not able to observe improvements in the Rietveld refinements using two-phase models of $LaTaON_2$ and $La_2Mg(Mg_{1/3}Ta_{2/3})O_6$. Nevertheless, we cannot rule out the presence of a miscibility gap in the phase diagram. Due to the peak broadening observed in the intermediate members of the solid solution the structural analysis was limited to determination of the unit cell dimensions using

Table 3
Lattice constants of $LaMg_xTa_{1-x}O_{1+3x}N_{2-3x}$ compounds

	$La_2Mg(Mg_{1/3}Ta_{2/3})O_6$	$LaMg_{1/2}Ta_{1/2}O_{5/2}N_{1/2}$	$LaMg_{1/3}Ta_{2/3}O_2N$	$LaTaON_2$
Refinement	Rietveld	Le Bail	Le Bail	Rietveld
S. G.	$P2_1/n$	$P2_1/n$	$P2_1/n$	$C2/m$
Z	2	4	4	4
V (Å^3)	253.496(6)	258.76(3)	260.90(2)	264.305(7)
a (Å)	5.61572(5)	5.6678(4)	5.7122(4)	8.0881(3)
b (Å)	5.66930(1)	5.6618(4)	5.6889(5)	8.0670(2)
c (Å)	7.96227(7)	8.0639(4)	8.0287(5)	5.7109(1)
β (°)	89.988(3)	89.476(3)	89.81(1)	134.820(1)

the Le Bail method of whole pattern fitting [62]. Table 3 compares the lattice constants of $LaMg_xTa_{1-x}O_{1+3x}N_{2-3x}$ compositions with $x = 0$, $\frac{1}{3}$, $\frac{1}{2}$, and $\frac{2}{3}$. The lattice volume in $LaMg_xTa_{1-x}O_{1+3x}N_{2-3x}$ increases regularly as the Ta- and N-content increases.

In the oxide lattice, the charge and size differences between Mg^{2+} and Ta^{5+} lead to a strong preference for site-ordering as is observed in ALaMgTaO$_6$ (A = Ba, Sr, Ca) and $La_2Mg(Mg_{1/3}Ta_{2/3})O_6$ perovskites [61]. But unlike those closely related oxide derivatives, $LaMg_{1/2}Ta_{1/2}O_{5/2}N_{1/2}$ and $LaMg_{1/3}Ta_{2/3}O_2N$ show only partially ordered Mg^{2+}/Ta^{5+} distributions. By comparing the peak areas for $d \approx \sqrt{4/3}a_p$ and $d \approx \sqrt{1/2}a_p$ diffractions, the long-range order parameters [63] of octahedral sites in $LaMg_{1/2}Ta_{1/2}O_{5/2}N_{1/2}$ and $LaMg_{1/3}Ta_{2/3}O_2N$ could be estimated as 24% and 7%, respectively. Such distinct Mg^{2+}/Ta^{5+} ordering behaviors in oxides and oxynitrides are attributable to the different anion environments in these two compound types. Unlike oxide perovskites, in oxynitrides the distribution patterns of complex cations and anions are interrelated. Although it is not possible to directly assess the O^{-2}/N^{-3} ordering with XRPD, it is quite probable that anion disorder accompanies, even facilitates, the cation disorder.

During the refinements of the profile parameters for $LaMg_xTa_{1-x}O_{1+3x}N_{2-3x}$ phases, the Gaussian term U was found to be abnormally large, implying substantial amounts of strain contributions to the peak broadening. This result taken in conjunction with the broad optical absorption edges (shown below), suggests variations in composition among the individual crystallites in $LaMg_xTa_{1-x}O_{1+3x}N_{2-3x}$ samples. The complex oxynitrides prepared in this work have compositions that can be achieved from the solid solution between a simple oxynitride perovskite and a complex oxide perovskite,

$$LaMg_xTa_{1-x}O_{1+3x}N_{2-3x} = (1-3x/2)LaTaON_2 + (3x)La_2Mg(Mg_{1/3}Ta_{2/3})O_6$$

$$BaSc_xTa_{1-x}O_{2+2x}N_{1-2x} = (1-2x)BaTaO_2N + (x)Ba_2ScTaO_6$$

The diagrams shown in Fig. 3 describe the correlations among the cation, anion compositions and crystal structures in the Ba–Sc–Ta–O–N and La–Mg–Ta–O–N systems. The compositions on the left legs represent solid solutions of $BaSc_xTa_{1-x}O_{2+2x}N_{1-2x}$ or $LaMg_xTa_{1-x}O_{1+3x}N_{2-3x}$ where the composition can vary smoothly while maintaining the ABX_3 perovskite stoichiometry. The observed XRPD data and optical spectra suggest that a finite range

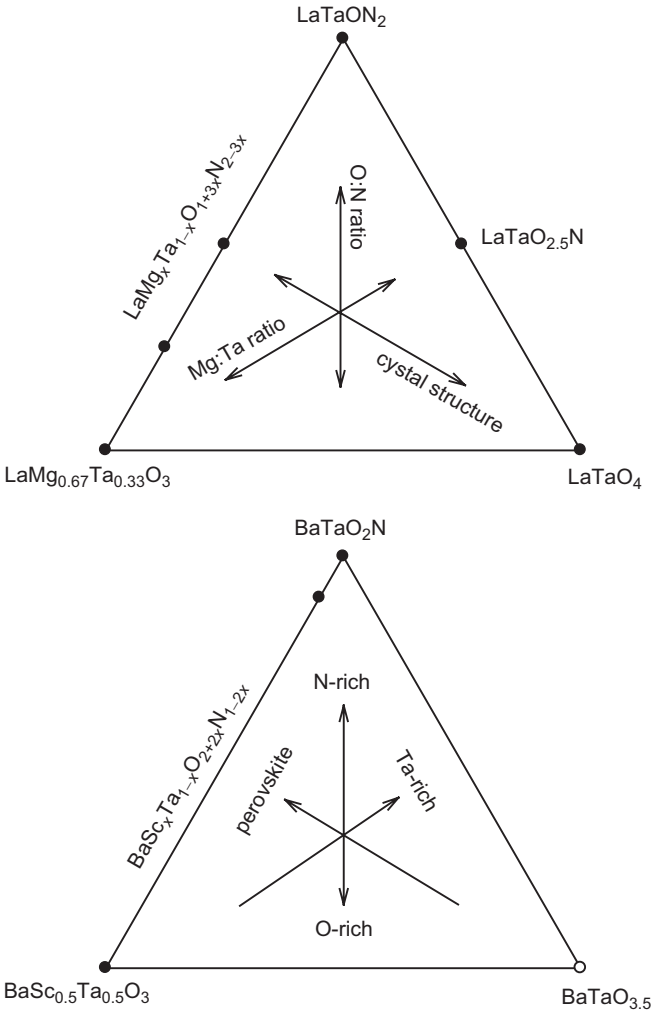

Fig. 3. Relations among the composition and crystal structure in the quaternary La–Mg–Ta–O–N and Ba–Sc–Ta–O–N systems. $LaTaO_4$ and $La_2Ta_2O_5N_2$ have $LaTaO_4$- and pyrochlore-type structures, respectively, whereas a single phase $Ba_2Ta_2O_7$ has not been reported.

of compositions are realized across the bulk sample. It would be interesting to see if a sol–gel precursor route would produce samples with increased homogeneity. However, such routes are not easily adapted to synthesis of compounds containing the Ta^{5+} ion.

3.3. Band gaps and sample colors

The complex perovskite oxynitrides exhibited slightly lighter colors compared to the simple perovskite oxynitrides containing Ta^{5+} as the single octahedral cation ($BaSc_{0.05}Ta_{0.95}O_{2.1}N_{0.9}$ vs. $BaTaO_2N$, $LaMg_xTa_{1-x}O_{1+3x}N_{2-3x}$ vs. $LaTaON_2$). From the UV–visible absorption spectra (Fig. 4), band gaps (E_g) are estimated as 1.8 eV for $BaSc_{0.05}Ta_{0.95}O_{2.1}N_{0.9}$ and 1.9 eV for $LaMg_{1/3}Ta_{2/3}O_2N$ and $LaMg_{1/2}Ta_{1/2}O_{5/2}N_{1/2}$. These values do not deviate much from the band gaps of $BaTaO_2N$ ($E_g = 1.8$ eV) [8] and $LaTaON_2$ ($E_g = 1.9$ eV) [61], respectively. This behavior is dissimilar to the trends found in the complex oxide perovskites [61]. However from the examination of the absorption spectra it is apparent that the complex oxynitrides have broader transitions at the absorption edges, which implies that there are manifold excitation paths with dispersed transition energies. It can be assumed that compositional variations in the sub-micrometer or nanometer scales render non-uniform absorption processes. The Sc- or Mg-rich domains will have larger band gap energies, whereas the Ta-rich part will have the band gaps closer to those of simple perovskites.

In Fig. 5, the band gaps of various perovskites with Ta^{5+}, Nb^{5+}, and Ti^{4+} are compared. Complex oxides have the largest band gaps (4.2–5.0 eV) and in a second group simple oxides and oxyfluorides have somewhat smaller band gaps (3.2–4.0 eV). Oxynitrides, whether they are of simple or complex type, have the band gaps of 1.7–2.4 eV. These values fall in the visible range of the electromagnetic spectrum, which explains the different colors displayed in Fig. 5. In general the Ta compounds have larger band gaps than Nb or Ti analogues. The Ta/M' ordering in oxides seems to widen the band gap by as much as ~1 eV. There are also minor variations of band gaps related to the structural distortions. However, the anion composition has the greatest impact on the band gap energy.

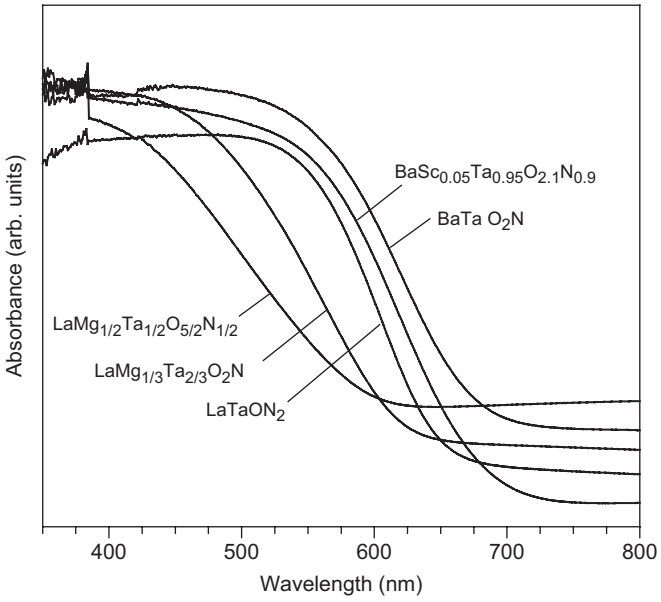

Fig. 4. UV–visible absorption spectra for complex perovskite oxides and oxynitrides.

In view of pigment applications, the visual sample colors are of practical importance. As can be seen from Fig. 5, the color of the oxynitrides can be widely tuned by adjusting the *A*- or *B*-site cations, and in certain cases the O/N ratio. It is also noted that even a minor composition control can cause significant modifications in the chromatic details of the product oxynitride. $BaSc_{0.05}Ta_{0.95}O_{2.1}N_{0.9}$ presents a brighter red color than $BaTaO_2N$, presumably due to the reduced sub-band gap transitions in the former (compare the baseline levels of UV–visible spectra in Fig. 4). While $LaTaON_2$ is deep red, $LaMg_{1/3}Ta_{2/3}O_2N$ and $LaMg_{1/2}Ta_{1/2}O_{5/2}N_{1/2}$ have lighter colors of a brilliant orange and a light ocher, respectively. It is expected that the colorimetric properties of perovskite oxynitrides would be further optimized by exploratory formulations of *A*- and *B*-site cations, although it may require exhaustive searches.

3.4. Dielectric properties

In a related study, the complex perovskite oxides $La_2Mg(Mg_{1/3}Ta_{2/3})O_6$ and Ba_2ScTaO_6 have been characterized as paraelectrics with the relative permittivity (κ) of 20–30 [61]. Through the conversion of oxide to oxynitride, there is the possibility that the increased covalency of the metal-nitrogen bonds (with respect to metal-oxygen bonds) may lead to dramatic changes in dielectric properties. Although there are relatively few studies of the dielectric properties of oxynitride perovskites, those reported examples [8,12,50,52] are quite interesting. In addition, the evidence presented above suggesting different compositions at the grain boundaries could lead to the formation of internal insulating barrier structure [64–66].

The dielectric behaviors of complex oxynitrides were examined by impedance spectroscopy and analyzed using equivalent circuit refinement. Fig. 6 compares the impedance spectra of Ba_2ScTaO_6, $BaTaO_2N$, and $BaSc_{0.05}Ta_{0.95}O_{2.1}N_{0.9}$ measured at 24 °C between 1 and 10^7 Hz. Most of electrical phenomena within the solid-state system can be monitored in the above frequency range, and hence the oxide Ba_2ScTaO_6 can be modeled as the parallel connection of a resistor and a constant phase element [56]. However the spectra of the oxynitride samples consist of two separate semicircles, one at higher frequency associated with bulk component and the other at lower frequency with grain boundary. The grain boundary contribution in oxynitrides becomes significant possibly

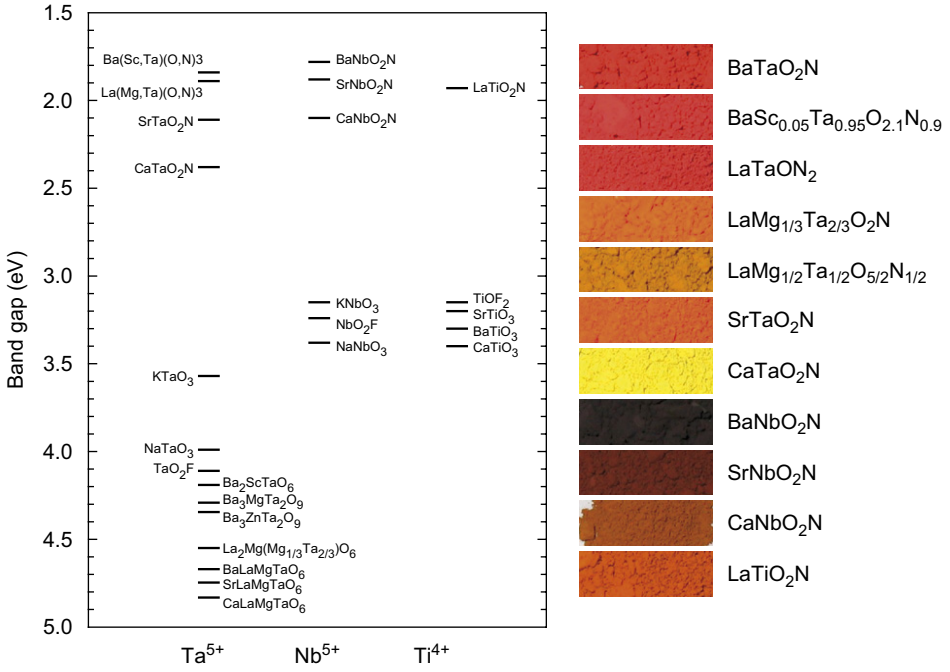

Fig. 5. Band gaps of various perovskites having Ta^{5+}, Nb^{5+}, or Ti^{4+} as the octahedral atom. Oxynitrides have the colors shown on the right, whereas all the oxides and oxyfluorides are white.

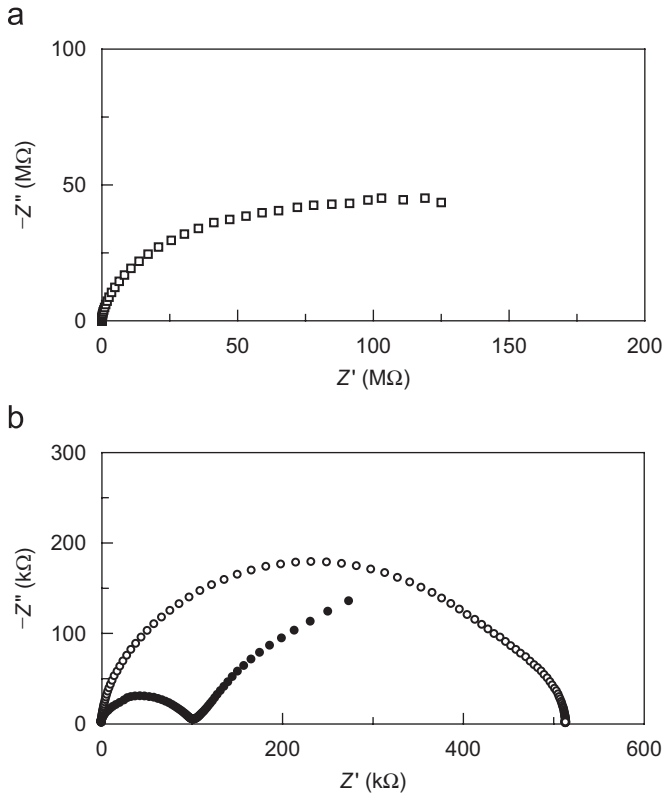

Fig. 6. Complex impedance spectra measured for (a) Ba_2ScTaO_6 (open squares), and (b) oxynitrides $BaSc_{0.05}Ta_{0.95}O_{2.1}N_{0.9}$ (filled circles) and $BaTaO_2N$ (open circles), at room temperature and $1–10^7$ Hz. Sample dimensions are ~0.05 cm^2 area by ~0.5 cm thickness. Note the different impedance units in both panels.

Table 4
Relative permittivities and conductivities of bulk and grain boundary components in complex perovskite oxynitrides at room temperature

	Bulk		Grain boundary	
	σ_{el} (S/cm)	κ	σ_{el} (S/cm)	κ
$LaMg_{1/3}Ta_{2/3}O_2N$	1.5×10^{-6}	120	4.1×10^{-8}	3900
$LaMg_{1/2}Ta_{1/2}O_{5/2}N_{1/2}$	1.1×10^{-6}	150	7.3×10^{-8}	2400
$La_2Mg(Mg_{1/3}Ta_{2/3})O_6$	6.2×10^{-10}	23	–	
$BaTaO_2N$	1.1×10^{-5}	4870	3.3×10^{-5}	3.2×10^5
$BaSc_{0.05}Ta_{0.95}O_{2.1}N_{0.9}$	8.5×10^{-6}	7300	6.6×10^{-7}	4.9×10^7
Ba_2ScTaO_6	9.0×10^{-9}	34	–	

due to the low packing density of the sample pellets (~55%) compared to those of oxides (~80%). It is worthy to mention that the two semicircles on the impedance plane are separated farther in $BaSc_{0.05}Ta_{0.95}O_{2.1}N_{0.9}$ than in $BaTaO_2N$ [8], which practically translates to the more resistive and capacitive grain boundary components in the former.

For the three complex oxynitrides, electrical conductivities and dielectric constants of bulk and grain boundary components have been evaluated by non-linear least squares refinement of impedance spectra as given in Table 4. For both the La- and Ba-containing compounds dielectric constants are significantly enhanced from those of oxide analogues, although the increments are relatively smaller in the La-compounds [61]. The loss $\tan\delta$ of

complex oxynitride samples are rather high, ~0.1 at 100 kHz.

The bulk electrical properties of $BaSc_{0.05}Ta_{0.95}O_{2.1}N_{0.9}$ are quite similar to that of $BaTaO_2N$ [8] but in the grain boundary part there is a remarkable difference. Upon introducing Sc, the resistivity and the capacity increased by ~2 orders at the grain boundary region, indicative of a chemical modification at the grain surface. Normally the extrinsic factors related with sample processing do not increase the resistance and capacitance simultaneously. Based on the XRPD analysis, the bulk phase of $BaSc_{0.05}Ta_{0.95}O_{2.1}N_{0.9}$ is assumed very close to $BaTaO_2N$ that implies that the grain boundary is formed of a Sc-containing oxide like $BaSc_2O_4$. Such a core/shell type heterogeneity in the microstructure resembles the internal barrier layer capacitor (IBLC) model suggested for perovskite oxides $CaCu_3Ti_4O_{12}$, $BaTiO_3$, and $Ca_{1-x}La_xMnO_3$ [64–66].

4. Conclusion

Quaternary complex perovskite oxynitrides have been explored in $La(Mg,Ta)(O,N)_3$ and $Ba(Sc,Ta)(O,N)_3$ systems. Ammonolyses using cation ratios of La:Mg:Ta = 2:1:1 and 3:1:2 produced monoclinic $LaMg_{1/2}Ta_{1/2}O_{5/2}N_{1/2}$ and $LaMg_{1/3}Ta_{2/3}O_2N$ structures, which posses an $P2_1/n$ symmetry on average, as does $La_2Mg(Mg_{1/3}Ta_{2/3})O_6$. In those complex oxynitrides there are competing tendencies of Mg^{2+}/Ta^{5+} order and O^{-2}/N^{-3} disorder. In the complex oxide perovskites, Mg^{2+} and Ta^{5+} show a strong preference toward the rock-salt type ordering, but in the oxynitrides the long range Mg^{2+}/Ta^{5+} order is significantly reduced, presumably by the disordered O^{-2}/N^{-3} arrangement. The rock-salt type cation ordering does not distinguish the anion sites and will not directly affect the O^{-2}/N^{-3} ordering. Due to the prevailing cation disorder, the complex perovskite oxynitrides exhibit nearly the same band gap edges as those of simple perovskites but their absorption energies are more diffuse. Impedance spectroscopy reveals interesting capacitor geometry in $BaSc_{0.05}Ta_{0.95}O_{2.1}N_{0.9}$ in which the semiconducting oxynitride grains are surrounded by insulating secondary phases. Careful designs of insulating grain boundaries can be important routes to built-in boundary layer capacitor architectures and/or better-improved chemical stability of oxynitride perovskite pigments.

Acknowledgments

The authors acknowledge funding from the National Science Foundation through the Center for the Design of Materials (CHE-043567) and a Materials World Network Grant (DMR-0603128).

References

[1] M. Almamouri, P.P. Edwards, C. Greaves, M. Slaski, Nature 369 (1994) 382.
[2] C.-Q. Jin, X.-J. Wu, P. Laffez, T. Tatsuki, T. Tamura, S. Adachi, H. Yamauchi, N. Koshizuka, S. Tanaka, Nature 375 (1995) 301.
[3] J.J. Pitha, A.L. Smith, R. Ward, J. Am. Chem. Soc. 69 (1947) 1870.
[4] O. Tougait, J.A. Ibers, Chem. Mater. 12 (2000) 2653.
[5] R. Asahi, T. Morikawa, T. Ohwaki, K. Aoki, Y. Taga, Science 293 (2001) 269.
[6] M. Jansen, H.P. Letschert, Nature 404 (2002) 980.
[7] D.P. Norton, Y.W. Heo, M.P. Ivill, K. Ip, S.J. Pearton, M.F. Chisholm, T. Steiner, Mater. Today 7 (2004) 34.
[8] Y.-I. Kim, P.M. Woodward, K.Z. Baba-Kishi, C.-W. Tai, Chem. Mater. 16 (2004) 1267.
[9] R.D. Shannon, Acta Crystallogr. A 32 (1976) 751.
[10] R. Marchand, F. Pors, Y. Laurent, Rev. Int. Hautes Temper. Refract. Fr. 23 (1986) 11.
[11] F. Pors, R. Marchand, Y. Laurent, P. Batcher, G. Roult, Mater. Res. Bull. 23 (1988) 1447.
[12] R. Marchand, F. Pors, Y. Laurent, O. Regreny, J. Lostec, J.M. Haussonne, J. de Phys. C 1 (1986) 901.
[13] S.J. Clarke, K.A. Hardstone, C.W. Michie, M.J. Rosseinsky, Chem. Mater. 14 (2002) 2664.
[14] E. Gunther, R. Hagenmayer, M. Jansen, Z. Anorg. Allg. Chem. 626 (2000) 1519.
[15] F. Pors, P. Bacher, R. Marchand, Y. Laurent, G. Roult, Rev. Int. Hautes Temper. Refract. Fr. 24 (1987–1988) 239.
[16] R. Marchand, F. Pors, Y. Laurent, Ann. Chim. Fr. 16 (1991) 553.
[17] J. Rooke, M. Weller, Solid State Phenom 90 (2003) 417.
[18] S.M. Ji, P.H. Borse, H.G. Kim, D.W. Hwang, J.S. Jang, S.W. Bae, J.S. Lee, Phys. Chem. Chem. Phys. 7 (2005) 1315.
[19] S.J. Clarke, B.P. Guinot, C.W. Michie, M.J.C. Calmont, M.J. Rosseinsky, Chem. Mater. 14 (2002) 288.
[20] J. Grins, G. Svensson, Mater. Res. Bull. 29 (1994) 801.
[21] M.T. Weller, S.J. Skinner, Int. J. Inorg. Mater. 2 (2000) 463.
[22] I.D. Fawcett, K.V. Ramanujachary, M. Greenblatt, Mater. Res. Bull. 32 (1997) 1565.
[23] G. Liu, X. Zhao, H.A. Eick, J. Alloys Compds. 187 (1992) 145.
[24] P. Bacher, P. Antoine, R. Marchand, P. L'Haridon, Y. Laurent, G. Roult, J. Solid State Chem. 77 (1988) 67.
[25] P. Antoine, R. Marchand, Y. Laurent, C. Michel, B. Raveau, Mater. Res. Bull. 23 (1988) 953.
[26] R. Pastrana-Fabregas, J. Isasi-Marin, C. Cascales, R. Saez-Puche, J. Solid State Chem. 180 (2007) 92.
[27] P. Antoine, R. Assabaa, P. L'Haridon, R. Marchand, Y. Laurent, Mater. Sci. Eng. B 5 (1989) 43.
[28] F. Pors, R. Marchand, Y. Laurent, J. Solid State Chem. 107 (1993) 39.
[29] P. Maillard, F. Tessier, E. Orhan, F. Chevire, R. Marchand, Chem. Mater. 17 (2005) 152.
[30] G.M. Veith, M. Greenblatt, M. Croft, J.B. Goodenough, Mater. Res. Bull. 36 (2001) 1521.
[31] M.J. Martinez-Lope, M.T. Casais, J.A. Alonso, Z. Naturforsch. B 61 (2006) 164.
[32] F. Pors, R. Marchand, Y. Laurent, Ann. Chim. Fr. 16 (1991) 547.
[33] N. Diot, R. Marchand, J. Haines, J.M. Légar, P. Macaudiere, S. Hull, J. Solid State Chem. 146 (1999) 390.
[34] R. Assabaa-Boultif, R. Marchand, Y. Laurent, J.-J. Videau, Mater. Res. Bull. 29 (1994) 667.
[35] G. Tobias, J. Oro-Sole, D. Beltran-Porter, A. Fuertes, Inorg. Chem. 40 (2001) 6867.
[36] J. Grins, P.O. Kall, G. Svensson, J. Solid State Chem. 117 (1995) 48.
[37] O. Morey, P. Goeuriot, J. Eur. Ceram. Soc. 25 (2005) 501.
[38] D. Berthebaud, F. Grasset, V. Allegret-Maret, S. Ababou-Girard, S. Pechev, J. Phys. Chem. C 111 (2007) 7883.

[39] Y. Laurent, R. Pastuszak, P. L'Haridon, R. Marchand, Acta Crystallogr. B 38 (1982) 914.
[40] P. L'Haridon, R. Pastuszak, Y. Laurent, J. Solid State Chem. 43 (1982) 29.
[41] F. Chevire, F. Tessier, R. Marchand, Mater. Res. Bull. 39 (2004) 1091.
[42] S.H. Elder, F.J. DiSalvo, J.B. Parise, J.A. Hriljac, J.W. Richardson Jr., J. Solid State Chem. 108 (1994) 73.
[43] N. Arumugam, A. Hönnerscheid, M. Jansen, Z. Anorg. Allg. Chem. 629 (2003) 939.
[44] H. Yamane, F.J. DiSalvo, J. Alloys Compds. 234 (1996) 203.
[45] P.S. Herle, M.S. Hegde, G.N. Subbanna, J. Mater. Chem. 7 (1997) 2121.
[46] R. Pastuszak, P. L'Haridon, R. Marchand, Y. Laurent, Acta Crystallogr. B 38 (1982) 1427.
[47] S.J. Clarke, P.R. Chalker, J. Holman, C.W. Michie, M. Puyet, M.J. Rosseinsky, J. Am. Chem. Soc. 124 (2002) 3337.
[48] M.-W. Lumey, R. Dronskowski, Z. Anorg. Allg. Chem. 631 (2005) 887.
[49] European Economic Community Guideline No. 91/338/ewg (1991).
[50] Y.-I. Kim, W. Si, P.M. Woodward, E. Sutter, S. Park, T. Vogt, Chem. Mater. 19 (2007) 618.
[51] B. Ravel, Y.-I. Kim, P.M. Woodward, C.M. Fang, Phys. Rev. B 73 (2006) 184121.
[52] Y.-I. Kim, P.M. Woodward, Ceram. Trans. 169 (2005) 179.
[53] A.C. Larson, R.B. von Dreele, General Structure Analysis System (GSAS), Report LAUR 86-748, Los Alamos National Laboratory, NM, 1994.
[54] B.H. Toby, J. Appl. Cryst. 34 (2001) 210.
[55] I.P. Shapiro, Opt. Spektrosk. 4 (1958) 256.
[56] J.R. Macdonald, Impedance Spectroscopy, Wiley, New York, 1987.
[57] M.T. Anderson, K.R. Poeppelmeier, Chem. Mater. 3 (1991) 476.
[58] P.W. Barnes, M.W. Lufaso, P.M. Woodward, Acta Crystallogr. B 62 (2006) 384.
[59] M.W. Lufaso, P.W. Barnes, P.M. Woodward, Acta Crystallogr. B 62 (2006) 397.
[60] C.J. Howard, B.J. Kennedy, P.M. Woodward, Acta Crystallogr. B 59 (2003) 463.
[61] Y.-I. Kim, Dissertation, The Ohio State University, USA, 2005.
[62] A. Le Bail, H. Duroy, J.L. Fourquet, Mater. Res. Bull. 23 (1988) 447.
[63] B.E. Warren, X-ray Diffraction, Dover Publications, New York, 1990, pp. 206–216.
[64] D.C. Sinclair, T.B. Adams, F.D. Morrison, A.R. West, Appl. Phys. Lett. 80 (2002) 2153.
[65] A.R. West, T.B. Adams, F.D. Morrison, D.C. Sinclair, J. Eur. Ceram. Soc. 24 (2004) 1439.
[66] J.L. Cohn, M. Peterca, J.J. Neumeier, J. Appl. Phys. 97 (2005) 034102.